Differential antiangiogenic and anticancer activities of the active metabolites of ginsenoside Rg3

AUTHOR(S)

Maryam Nakhjavani, E Smith, K Yeo, Y Tomita, T J Price, A Yool, A R Townsend, J E Hardingham

PUBLICATION DATE

03-06-2021

HANDLE

10536/DRO/DU:30159026

Journal of Ginseng Research xxx (xxxx) xxx

Contents lists available at ScienceDirect

Journal of Ginseng Research

journal homepage: www.ginsengres.org

Research Article

Differential antiangiogenic and anticancer activities of the active metabolites of ginsenoside Rg3

Maryam Nakhjavani [a], Eric Smith [a, b, *], Kenny Yeo [a, b], Yoko Tomita [a, b, c], Timothy J. Price [b, c], Andrea Yool [b], Amanda R. Townsend [b, c], Jennifer E. Hardingham [a, b]

[a] Molecular Oncology, Basil Hetzel Institute for Translational Health Research, The Queen Elizabeth Hospital, Woodville South, SA, 5011, Australia
[b] Adelaide Medical School, University of Adelaide, Adelaide, SA, 5005, Australia
[c] Medical Oncology Unit, The Queen Elizabeth Hospital, Woodville South, SA, 5011, Australia

ARTICLE INFO

Article history:
Received 24 February 2021
Received in revised form
18 May 2021
Accepted 24 May 2021
Available online xxx

Keywords:
Anticancer
Epimer
Ginsenoside Rh2
Ginsenoside Rg3
Protopanaxadiol

ABSTRACT

Background: Epimers of ginsenoside Rg3 (Rg3) have a low bioavailability and are prone to deglycosylation, which produces epimers of ginsenoside Rh2 (S−Rh2 and R−Rh2) and protopanaxadiol (S-PPD and R-PPD). The aim of this study was to compare the efficacy and potency of these molecules as anti-cancer agents.

Methods: Crystal violet staining was used to study the anti-proliferatory action of the molecules on a human epithelial breast cancer cell line, MDA-MB-231, and human umbilical vein endothelial cells (HUVEC) and compare their potency. Cell death and cell cycle were studied using flow cytometry and mode of cell death was studied using live cell imaging. Anti-angiogenic effects of the drug were studied using loop formation assay. Molecular docking showed the interaction of these molecules with vascular endothelial growth factor receptor-2 (VEGFR2) and aquaporin (AQP) water channels. VEGF bioassay was used to study the interaction of Rh2 with VEGFR2, *in vitro*.

Results: HUVEC was the more sensitive cell line to the anti-proliferative effects of S−Rh2, S-PPD and R-PPD. The molecules induced necroptosis/necrosis in MDA-MB-231 and apoptosis in HUVEC. S−Rh2 was the most potent inhibitor of loop formation. *In silico* molecular docking predicted a good binding score between Rh2 or PPD and the ATP-binding pocket of VEGFR2. VEGF bioassay showed that Rh2 was an allosteric modulator of VEGFR2. In addition, SRh2 and PPD had good binding scores with AQP1 and AQP5, both of which play roles in cell migration and proliferation.

Conclusion: The combination of these molecules might be responsible for the anti-cancer effects observed by Rg3.

1. Introduction

Ginsenoside Rg3 (Rg3) is one of the best studied members of the ginsenoside family of molecules extracted from *Panax ginseng*. Like other ginsenosides, Rg3 has two epimers; 20(S)-ginsenoside Rg3 (SRg3) and 20(R)-ginsenoside Rg3 (RRg3). Several studies have reported the anticancer properties of the Rg3 epimers (reviewed in [1,2]). Orally administered Rg3 is a registered drug in China [3] and has been evaluated in clinical trials as a single drug for lung [4] and liver cancer [5] or in combination with standard chemotherapies [3,6]. However, animal studies have suggested that extensive metabolism of Rg3 occurs in the gastrointestinal tract (reviewed in [1]). For example, the bioavailability of Rg3 in rats was less than 3% [7]. This suggests that Rg3 metabolites could contribute to the efficacy of Rg3. Deglycosylation of Rg3 epimers is an important metabolic pathway, which leads to formation of the active metabolites; ginsenoside Rh2 (Rh2) and protopanaxadiol (PPD) [8] (Fig. 1).

Our group has been interested in finding novel treatments for metastatic triple-negative breast cancer patients. We have shown the stereoselective activities of SRg3 and RRg3 in inhibition of the proliferation, migration and invasion of triple negative breast cancer cell lines [9] and have demonstrated the efficacy of these epimers in inhibition of angiogenesis, *in vitro* [10]. Using *in silico*

* Corresponding author. Molecular Oncology, Basil Hetzel Institute for Translational Health Research, The Queen Elizabeth Hospital, Woodville South, SA, 5011, Australia.
E-mail address: eric.smith@adelaide.edu.au (E. Smith).

https://doi.org/10.1016/j.jgr.2021.05.008

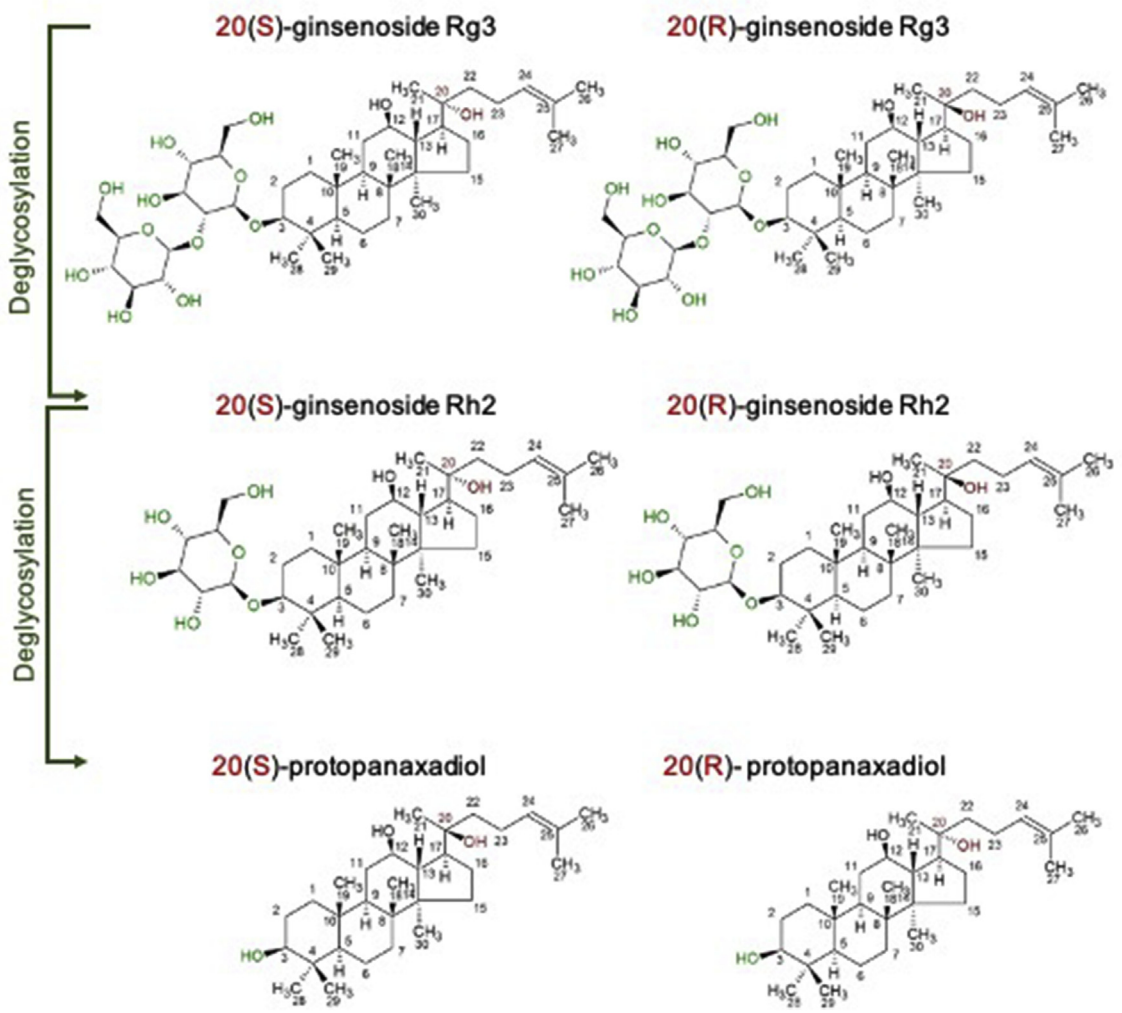

Fig. 1. The structure of epimers of ginsenoside Rg3 and their metabolites. Deglycosylation of 20(S)- and 20(R)-ginsenoside Rg3 produces 20(S)- and 20(R)-ginsenoside Rh2 and 20(S)- and 20(R)-protopanaxadiol. The stereocenter on C_{20} is highlighted with a red color and heteroatoms of the sugar molecules are shown in green.

molecular docking and the frog oocyte swelling assay, we showed only SRg3, stereoselectively, blocked the water transport function of aquaporin 1 (AQP1) [9]. AQP1 plays important roles in cell proliferation, migration, invasion and angiogenesis (reviewed in [2,11]).

Continuing with the screening of ginsenosides as potential treatment options for metastatic triple-negative breast cancer breast cancer, the aim of the current research was to investigate the antiangiogenic and anticancer properties of the Rh2 and PPD epimers, as potentially active, clinically relevant metabolites of Rg3. To investigate the differential effects of these epimers, a human triple-negative breast cancer cell line (MDA-MB-231) and non-transformed normal endothelial cells (HUVEC) were considered to compare the efficacy of these epimers as both anticancer and antiangiogenic agents, *in vitro*. The effects of these epimers on proliferation and mode of cell death in both cell types are studied and potential anti-angiogenic mechanisms are discussed.

2. Materials and methods

2.1. Cell lines, reagents and cell culture

MDA-MB-231 was purchased from American Type Culture Collection (ATCC; Manassas, VA, USA) and grown as previously described [9]. HUVEC and its media, EBM-2 Endothelial Cell Growth Medium-2 were both from Lonza (Lonza, Basel, Switzerland). 20(S)- and 20(R)- epimers of ginsenoside Rh2 and protopanaxadiol were from ChemFaces Biochemical Co. (Wuhan, China). Drugs were dissolved in dimethyl sulfoxide (DMSO D2650, HYBRI-MAX, Sigma-Aldrich, St Louis, MO, USA). Aliquots of 25 mM of the molecules were kept at −20°C. Concentrations of 0-100 μM of ginsenosides was used with maximum of 0.2% DMSO as the vehicle control. Cell lines were mycoplasma-free, as determined using the MycoAlert Detection Kit (Lonza) and/or a custom PCR-based assay, as described previously [12,13].

2.2. Proliferation assay

To test the efficacy of the ginsenosides on cell proliferation, crystal violet assay (CVA) was used, as previously described [9]. Briefly, MDA-MB-231 and HUVEC cells were seeded at 3×10^3 and 0.8×10^3 cells/well of 96-well plates. On days 0, 1 and 3, CVA was performed, and the absorbance of each well was read using FLUOstar Optima microplate reader (BMG Labtech, Offenburg, Germany) at 595 nm. The experiment included 6 replicates. The data are shown as mean ± standard deviation (SD).

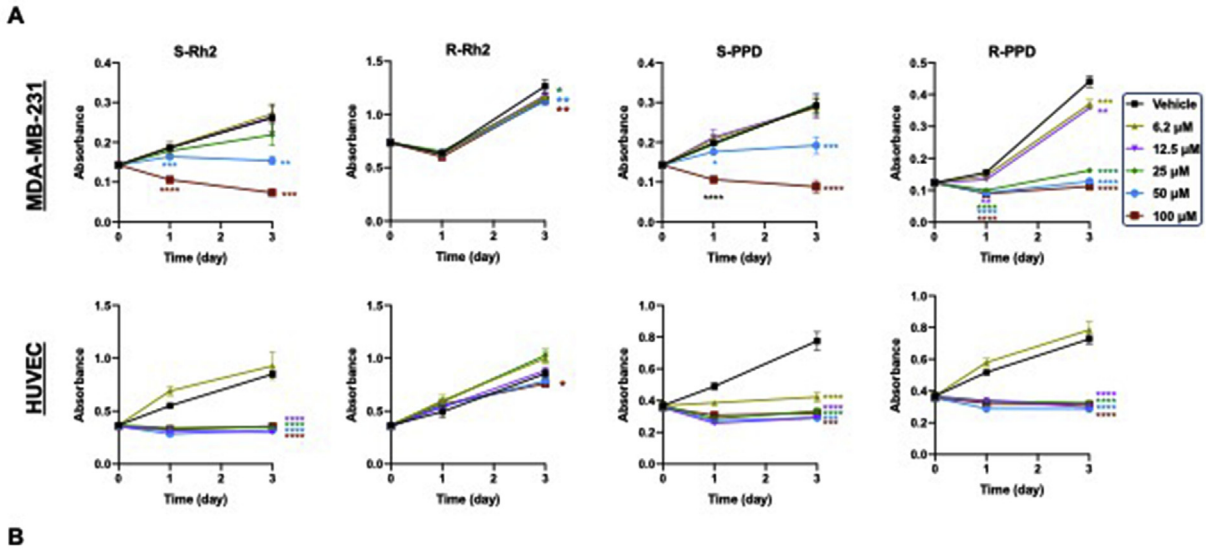

B

	IC_{50} (μM) (95% log confidence interval)		
	S-Rh2	S-PPD	R-PPD
MDA-MB-231	59 (1.625-1.940)	50 (1.691-1.712)	16 (1.183-1.247)
HUVEC	9 (8.619-8.644)	5 (0.7334-0.7334)	9 (0.9696-0.9696)

Fig. 2. (**A**) Crystal violet assay on MDA-MB-231 and HUVEC cells exposed to 0-100 μM of S−Rh2, R−Rh2, S-PPD or R-PPD for up to 3 days. Each data point represents mean ± SD of 6 replicates. *p = 0.01, **p = 0.007, ***p < 0.001, ****p < 0.0001, (**B**) the calculated half-maximal inhibitory concentration (IC_{50}) causing reduced survival of MDA-MB-231 and HUVEC cells treated with S−Rh2, S-PPD or R-PPD, at 72 h.

2.3. Cell viability and half maximal inhibitory concentration (IC_{50}) calculation

Based on CVA data on day 3, cell viability and dose-response curves were plotted using non-linear regression using log(inhibitor) vs. normalized response using GraphPad Prism (version 9.0.0 for Mac, GraphPad Software, San Diego, California USA, www.graphpad.com) to calculate IC_{50}.

2.4. Loop formation assay

As previously described [14], 10 μL of Matrigel® (Corning® Matrigel® Basement Membrane Matrix, LDEV-free, cat# 354234, NY, USA) was used to coat each well of a Angiogenesis 96 Well μ-Plate (Ibidi, Martinsried, Germany). HUVEC was seeded at 1.5×10^4 cells/well and exposed to the vehicle or 1, 10, 50 and 100 μM of ginsenosides. The number of formed loops in each well was counted after 8 h. The experiment was performed in triplicate. The data are presented as mean ± SD.

2.5. Flow cytometric analysis of cell death and cell cycle

The assay was performed as previously described [9,15]. Briefly, MDA-MB-231 and HUVEC cells were seeded at 1×10^5 and 0.5×10^5 cells/well of six-well plates and incubated overnight and then exposed with the drugs or vehicle for 3 days. To analyse cell death, cells were harvested, stained using Annexin-V-FLUOS Staining Kit (Roche Diagnostics, Mannheim, Germany). To analyse cell cycle, the cells were harvested, washed and fixed for 2 h in an equal volume of 100% ice cold ethanol at −20°C. Then the cells were washed and resuspended in 100 μL of propidium iodide (PI) staining solution consisting of 25 μg/mL PI (Sigma-Aldrich, St Louis, MO, USA), 40 μg/mL bovine pancreas ribonuclease A (Sigma-Aldrich), and 0.25% Triton X-100 (Sigma-Aldrich). The cells were analysed using a BD FACSCanto II (BD Biosciences, San Jose, CA, USA), capturing 10,000 single cell events per sample. Data was analysed using FlowJo software v10.4.0 (FlowJo, LLC, Ashland, OR, USA). The experiment was performed in triplicate. The data are presented as mean ± SD. Sub-G1 population was considered as cell death. To calculate cell cycle arrest in each phase, sub-G1 population was excluded.

2.6. Studying mode of cell death using IncuCyte

MDA-MB-231 and HUVEC cells were seeded at 6.6×10^3 and 1.5×10^3 cells/well of 96-well flat-bottomed plates. Following an overnight incubation, the cells were treated with Rh2 and PPD epimers or vehicle, containing 1:1000 dilution of Caspase-3/7 Green Detection Reagent (CellEvent™, Thermo Fisher Scientific) to detect apoptosis. To detect necrosis, 2.5 μg/mL PI was used. Drozitumab 100 ng/mL and staurosporine 0.25 μM (Sigma-Aldrich) were used as positive controls for apoptosis in MDA-MB-231 and HUVEC, respectively [16,17]. Drozitumab was freshly prepared by combining equal volumes of 100 ng/μL of drozitumab (Genentech, South San Francisco, CA, USA) with 100 ng/μL of affinity purified goat anti-human IgG Fcγ fragment (Jackson Immunoresearch Laboratories West Grove, PA, USA), incubating for 30 min at 4° C, and then diluting in culture medium for a final concentration of 100 ng/mL of drozitumab [17]. The number of positive cells for activation of caspase 3/7 or staining with PI was determined using an IncuCyte S3 Live-Cell Analysis System (Sartorius, Goettingen, Germany), acquiring four images per well every 2 h for 48 h.

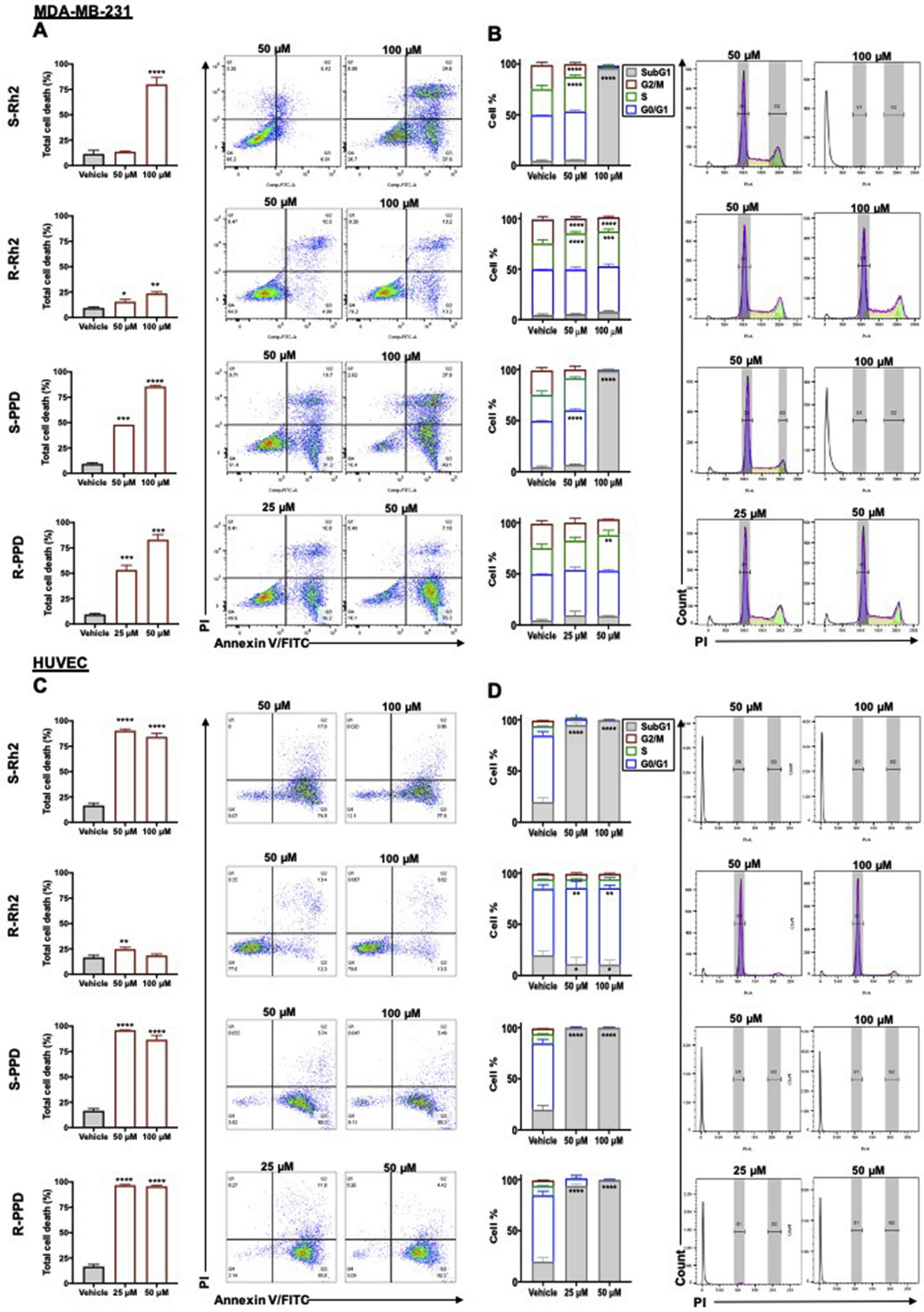

Fig. 3. Analysis of (**A**) cell death and (**B**) cell cycle arrest in MDA-MB-231 cell line and (**C**) cell death and (**D**) cell cycle arrest in HUVEC following a three-day exposure to S−Rh2, R−Rh2, S-PPD, and R-PPD. Each data point represents mean ± SD of three replicates. All comparisons are between the treatments and the vehicle control cells, $p < 0.05$.

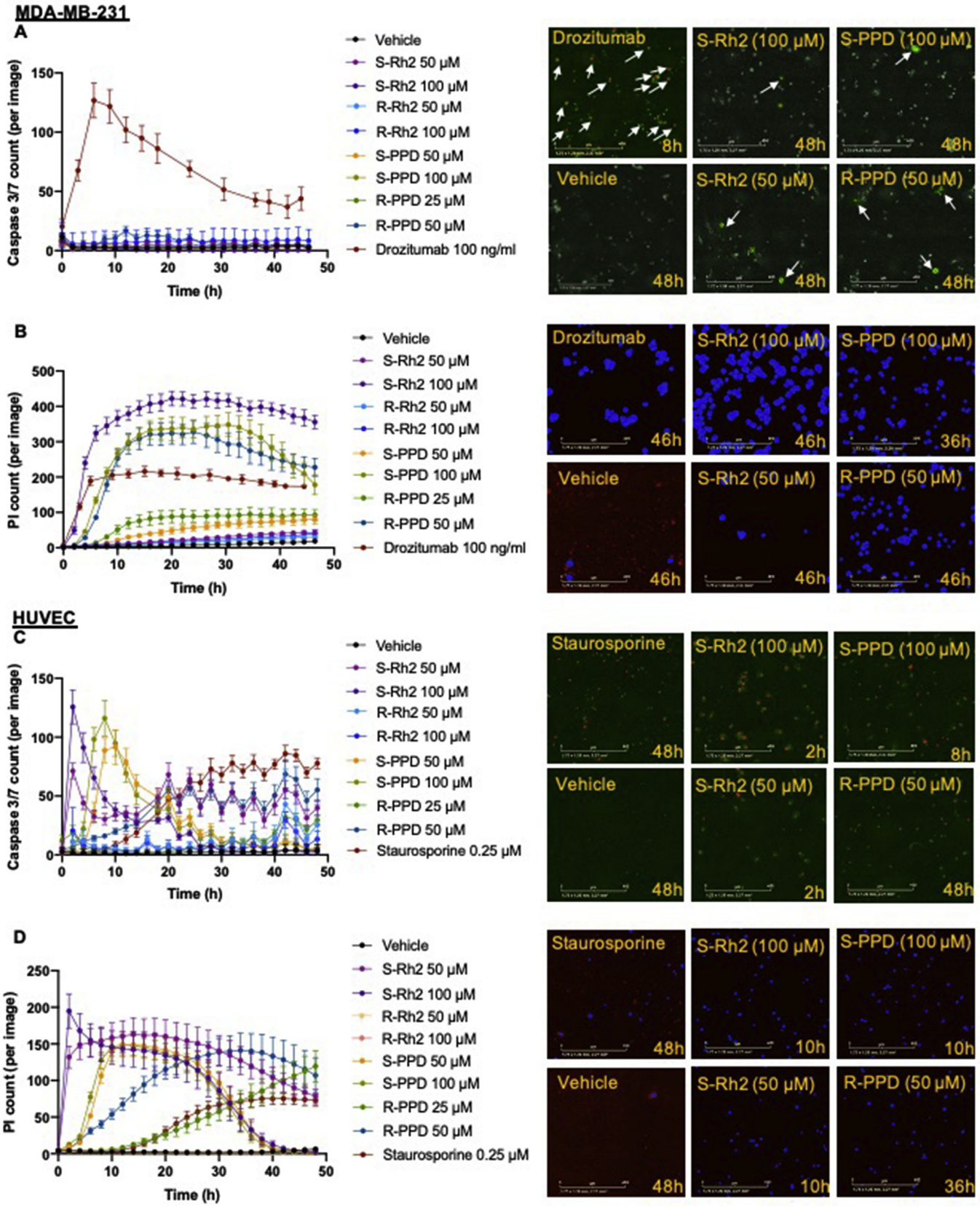

Fig. 4. Mode of cell death in MDA-MB-231 and HUVEC cells exposed to Rh2 and PPD epimers. (**A**) and (**C**) show activation of caspase 3/7 in MDA-MB-231 cells, and HUVEC respectively. White arrows pointing at red dots show activation of caspase 3/7 in cells. (**B**) and (**D**) show staining of cells PI in MDA-MB-231 and HUVEC cells, respectively. Blue spots indicate cells positive for PI. Staurosporine or drozitumab were used as positive controls. Scale bars show 400 μm. Each data point represents mean ± SD of 8 replicates.

2.7. Molecular docking

Crystal structures of VEGFR2 (2XIR and 3V2A), AQP1 (1FQY), AQP2 (4NEF), AQP4 (3GD8) and AQP5 (3D9S) were obtained from the protein data bank of NCBI (RCSB PDB). Canonical SMILES structures of Rh2 [18] and PPD [19] available on PubChem were used to prepare the 3D structure of each molecule in the UCSF Chimera program (version 1.15-mac64). The molecular docking was performed as previously described [9,20], using UCSF Chimera program and Autodock Vina algorithm (version 1.1.2_Mac_Catalina_64bit). The energies of interaction were predicted based on the flexible ligand docking simulations run within the docking grids on the intracellular side of the monomeric pores.

2.8. VEGF bioassay

VEGF Bioassay (Promega, Madison, WI, USA) was used to study the effects of S−Rh2 on the activation of VEGFR2. This bioluminescent kit includes KDR/NFAT-RE HEK293 cells, in which activation of VEGFR2 triggers NFAT-RE-mediated luminescence. According to the manufacturer's protocol, the cells were seeded in white, flat-bottom 96-well assay plates (Delta Surface ™, Thermo Scientific, Roskilde, Denmark). Cells received serial dilutions of S−Rh2 at a maximum final concentration of 100 μM, alone or in combination with VEGF-A (recombinant VEGF, Promega) at a constant final concentration of 35 ng/mL (80% effective concentration). Controls included bevacizumab and VEGF-A at the maximum final concentration of 6 μg/mL and 0.1 μg/mL, respectively. After 6 h of incubation, the cells were exposed to Bio-Glo™ Reagent, incubated for 10 minutes and then the luminescence was read using the Optima plate reader. The relative luminescence units (RLU) in each well were subtracted from the background. The experiment was performed in duplicate.

2.9. Statistical analysis

One-way or two-way analysis of variance (ANOVA) was performed using GraphPad Prism version 9.0.0 for Mac, GraphPad Software, San Diego, California USA, www.graphpad.com.

3. Results and discussion

3.1. Rh2 and PPD inhibit the proliferation of HUVEC and MDA-MB-231

The results of the anti-proliferative effects of epimers of Rh2 and PPD are shown in Fig. 2A, and the derived IC_{50} values are presented in Fig. 2B. Previous studies showed that S−Rh2 had efficacy against hematologic [21,22], colon [23] and prostate [24] cancer, *in vitro*. In our studies, S−Rh2 significantly inhibited proliferation at 50 μM ($p = 0.007$) and 100 μM ($p = 0.0009$) in MDA-MB-231, and at $\geq$ 12.5 μM ($p < 0.0001$) in HUVEC (Fig. 2A).

S−Rh2 seems to be the active form of Rh2 responsible for its anti-proliferative action in these cells, since R−Rh2 showed much less inhibitory action on MDA-MB-231 and HUVEC (Fig. 2A) and IC_{50} values could not be calculated for this molecule. Similar to our results, it was shown that R−Rh2 did not inhibit the proliferation of prostate cancer cell lines [24].

S-PPD was more effective on HUVEC than on MDA-MD-231. S-PPD $\geq$ 6.2 μM significantly inhibited the proliferation of HUVEC ($p \leq 0.0002$), while for MDA-MB-231, only 50 μM ($p = 0.0002$) and 100 μM ($p < 0.0001$) showed anti-proliferative action (Fig. 2A).

When comparing the PPD epimers, R-PPD was more potent than S-PPD on MDA-MB-231 (IC_{50} 16 μM [95%CI 15.24 to 17.65] versus 50 μM [95%CI 49.11 to 51.53], respectively). In contrast on HUVEC, S-PPD was more potent than R-PPD (IC_{50} 5 μM [95%CI 5.413 to 5.413] versus 9 μM [95%CI 9.324 to 9.324], respectively). The IC_{50} values of S-PPD and R-PPD on HUVEC are similar to previous reports [25].

In summary, these data demonstrate that HUVEC was more sensitive than MDA-MB-231 to the anti-proliferative effects of Rg3 metabolite epimers, S−Rh2, S-PPD and R-PPD. R−Rh2 had little effect on both cell lines, even at the highest concentration tested. In HUVEC, S−Rh2, S-PPD and R-PPD showed similar efficacies. In contrast, MDA-MB-231 was more sensitive to R-PPD than S−Rh2 and S-PPD. These *in vitro* findings raise the possibility that the clinically relevant target of the Rg3 metabolite epimers are the endothelial cells.

3.2. Rh2 and PPD epimers induce cell death and cell cycle arrest

To compare the anti-proliferative mechanisms of these molecules, the highest concentrations that were effective on both cell types were chosen. Fig. 3 shows the results of cell death and cell cycle arrest, and Fig. 4 shows the results of mechanism of cell death induced by these molecules. In MDA-MB-231, the pattern of distribution of dead cells was different from HUVEC. Although a high proportion of MDA-MB-231 and HUVEC cells were located in quadrant (Q) 3 of the flow cytometry plot, annexin V-positive, MDA-MB-231 cells also had a distinct population in Q2 annexin V-/PI-positive, late apoptosis or necroptosis/necrosis (Fig. 3). In these cells, 50 μM S−Rh2 did not induce cell death (Fig. 3A) but increased cell cycle arrest in S phase by 34% (Fig. 3B). At 100 μM ($p = 0.0004$), S−Rh2 induced approximately 80% cell death (Fig. 3A) and increased cell cycle arrest in S phase by 99% ($p < 0.0001$) in the remaining 20% cells (Supplementary Fig. 1). In a study performed by Choi et al (2009), a 48-h exposure to 40 μM Rh2 (unspecified epimer) caused a slight increase in G1 population of MCF-7 and MDA-MB-231 [26]. Their result may not be completely comparable with ours due to lack of specification of the epimer used and the difference in the exposure time. However, it is possible to conclude that in lower concentrations and shorter exposure times (such as 48 h), S−Rh2 might induce cell cycle arrest and this cell cycle arrest might lead to cell death in longer exposure times (such as 72 h in our experiment).

To determine mode of cell death, caspase 3/7 reagent was used to detect activation of apoptosis or with PI to detect loss of cell membrane integrity (Fig. 4). At 50 and 100 μM S−Rh2, no activation of caspase 3/7 was observed (Fig. 4A). In contrast, at 100 μM a rapid increase in PI staining was observed, consistent with the observed cell death. These findings suggest that the annexin V-positive MDA-MB-231 cells observed following S−Rh2 treatment are not due to induction of apoptosis but are likely to be the result of a loss in membrane integrity and induction of necroptosis/necrosis. Necroptosis is a caspases-independent programmed cell death, in which similar to apoptotic cells, phosphatidylserine in the cell membrane is flipped and cell rupture results in release of DAMPs recruiting immune cells to also prompt a non-inflammatory cell death [27,28]. *In vitro* and in the absence of immune cells and phagocytosis, cell membrane of late necroptotic cells becomes leaky and the cells become positive for both annexin V and PI [29]. Genotoxic stress and anti-cancer agents such as shikonin (the R enantiomer of alkanin) are also amongst the inducers of necroptosis [30]. Shikonin, was the first reported inducer of necroptosis [31,32], which was shown to overcome cancer drug resistance [32,33] and inhibit osteosarcoma-induced lung metastasis [34] via induction of necroptosis.

In HUVEC, 50 and 100 μM S−Rh2 rapidly (within 2 h) induced activation of caspase 3/7 (Fig. 4C) and loss of membrane integrity (Fig. 4D). The count of positively stained cells reduced over time, and examination of the images revealed that this was due to

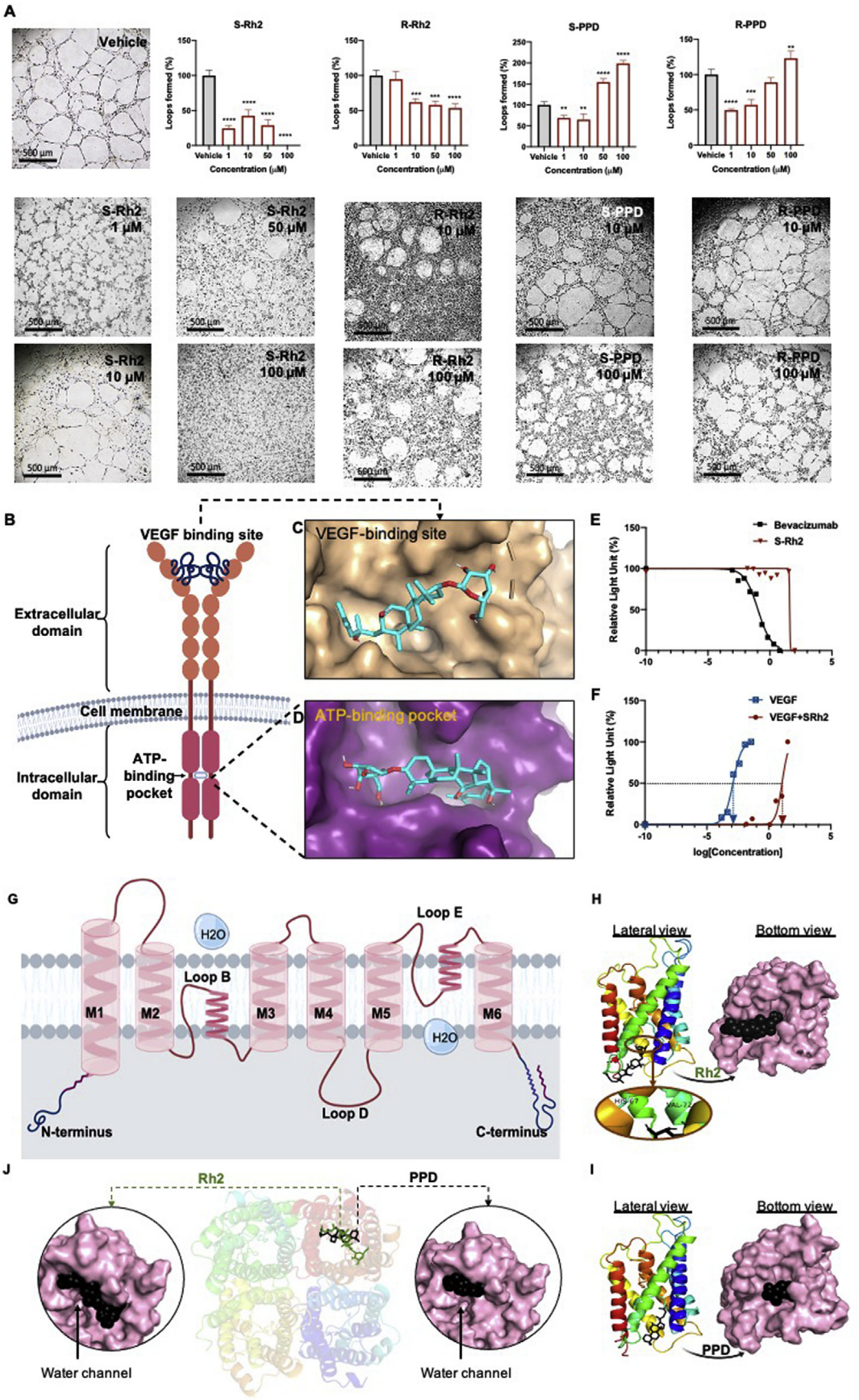

Fig. 5. (**A**) Loop formation assay in HUVEC cells following exposure to S−Rh2, R−Rh2, S-PPD, and R-PPD. Each data point represents mean ± SD of two or three replicates. All comparisons are between the treatments and the vehicle control cells, $p < 0.05$, (**B**) schematic structure of VEGFR2 showing the extracellular domain, VGEF binding site,

progressive disintegration of the positive cells. After 3 days of treatment the majority of the remaining cells (71% for 50 and 100 μM) were annexin V-positive/PI-negative (Fig. 3C). These remaining cells had arrested at S phase and the G2/M population had disappeared (Fig. 3D, Supplementary Fig. 1). Overall, results showed that S−Rh2 was an inducer of necroptosis/necrosis in MDA-MB-231 and apoptosis in HUVEC.

In both cell types, R−Rh2 caused a minimal inhibition of proliferation (Fig. 2), consistent with the results of annexin V/PI staining (Fig. 3) and mode of cell death (Fig. 4). R−Rh2 induced cell cycle arrest in S phase by about 40% ($p < 0.0001$) and in G0/G1 phase by about 3% ($p < 0.01$) in MDA-MB-231 and HUVEC, respectively, suggesting that cell cycle arrest is a dominant mechanism of this molecule in inhibition of proliferation (Fig. 3A and C).

In MDA-MB-231, 50 and 100 μM S-PPD induced a significant increase in the proportion of cells that stained annexin-positive (Fig. 3A), with no caspase 3/7 activation (Fig. 4A). Instead, it significantly increased the PI count within 4 h with 100 μM ($p < 0.0001$) and 12 h with 50 μM ($p = 0.0002$) (Fig. 4B), suggesting that it induced a necroptotic/necrotic cell death. In HUVEC, a significant increase in annexin V-positive/PI-negative cells (Fig. 3C), and an increase in the caspase 3/7-positive cell count, which peaked at 8 h with 100 μM and 10 h with 50 μM (Fig. 4C), was observed. The increase in the caspase 3/7 cell count was closely followed by a significant increase in PI-positive cell count (Fig. 4D). This confirms the finding of Wang et al showing induction of apoptosis by S-PPD. They suggested that high concentrations of S-PPD could be used for the treatment of angiogenesis-related diseases [35].

R-PPD was the most potent anti-proliferative molecule in MDA-MB-231 (Fig. 2B). At 25 μM ($p = 000.9$) and 50 μM ($p = 0.0001$), R-PPD, in a concentration-dependent manner, induced 53% and 83% cell death (Fig. 3A) and 30% cell cycle arrest in S phase (Supplementary Fig. 1). Similar to other studied epimers, R-PPD did not induce activation of caspase 3/7 in MDA-MB-231 (Fig. 4A), but increased PI staining, dose-dependently (Fig. 4B). This could indicate that R-PPD is also an inducer of necroptotic/necrotic cell death in this cell line. In HUVEC, R-PPD induced 95% cell death at both tested concentrations ($p < 0.0001$), and 15% cell cycle arrest in G0/G1 (Supplementary Fig. 1), accompanied by a gradual increase in caspase 3/7 activation and PI count, indicating apoptosis. Overall, these findings suggest that S−Rh2, S-PPD and R-PPD, at their highest concentrations studied, induced necroptosis/necrosis in MDA-MB-231 and induced apoptosis in HUVEC. These molecules induce S-phase arrest in MDA-MB-231 and G0/G1 arrest in HUVEC. To further study the anti-proliferative mechanisms of these epimers, studies on IC_{50} concentrations are suggested.

3.3. S−Rh2 is the most potent inhibitor of loop formation

Fig. 5 shows the results of loop formation assay. Vehicle treated HUVEC formed clear loops with elongated cells. Among the four tested molecules, S−Rh2 was the most potent in inhibiting loop formation. At 50 and 100 μM, cell migration was completely inhibited, and no loops were formed ($p < 0.0001$), which could be due to the rapid cell death induced by this drug (Fig. 4C and D). At lower concentrations of S−Rh2 loop formation was also significantly inhibited ($p < 0.0001$). This indicates that the mechanism by which S−Rh2 inhibits loop formation might be different at different concentrations. At 1 μM, though the concentration was very low, the cells made deformed and unusual loops. This low concentration, after two days of exposure, increased the activation of caspase 3/7 (Supplementary Fig. 2). At 10 μM no significant induction of cell death was observed in the cells (Supplementary Fig. 2) and the cells survived on Matrigel. It has been shown that 10 μM Rh2 (unspecified epimer) decreased the activation of GRB2-associated-binding protein 1 (Gab1), vascular endothelial growth factor receptor 2 (VEGFR2), protein kinase B (PKB or AKT) and extracellular signal-regulated kinase 1/2 (ERK 1/2) [36]. We showed that 10 μM S−Rh2 caused small levels of decrease in the expression of AQP1 and activation of focal adhesion kinase (FAK) (Supplementary Fig. 4), which could contribute to the anti-angiogenic properties of this drug (reviewed in [37]). Also, preliminary data show that at this concentration, S−Rh2 caused a non-significant reduction in the size of MDA-MB-231 mammospheres (Supplementary Fig. 5). This effect, which might indicate a looser cell-cell connection in these mammospheres, together with the anti-angiogenic effects of this S−Rh2, could contribute to the anti-cancer effects of this molecule.

R−Rh2 showed some level of inhibition of loop formation at 10 ($p = 0.0003$), 50 ($p = 0.0001$) and 100 μM ($p < 0.0001$), with no significant efficacy at 1 μM R. S-PPD and R-PPD showed a U-shaped dose-response curve in loop formation assay, showing inhibition of loop formation only in lower concentrations. This U-shaped dose-response curve was also reported for Rg3 epimers (reviewed in [2]). The observed effects on loop formation are a cells' immediate response to these agents. With pretreated cells, due to the significant anti-proliferative effects of the molecules, it is expected that the anti-loop formation effects of molecules be much increased. Therefore, it could be concluded that the molecules are potent anti-angiogenic agents. We also tested the anti-proliferative effects of these four molecules at nM and low μM ranges in HUVEC (Supplementary Fig. 3). Unlike the reported effects for Rg3 (reviewed in [2]), these molecules did not have anti-proliferative effects at such low concentrations in HUVEC, although, after 2 days exposure to 1 μM S−Rh2, evidence of activation of caspase 3/7 was observed (Supplementary Fig. 2).

Table 1
Binding Scores (Number of H Bonds) of Rh2 and PPD With Different Aquaporin Water Channels, ATP-Binding Pocket or the VEGF-Binding Site of VEGFR2.

Molecules	Binding score (kJ/mol) (number of H-bonding)					
	VEGFR2[a]	VEGFR2[b]	AQP1	AQP2	AQP4	AQP5
Rh2	−7.6 (1)	−7.1 (2)	−8.1 (2)	−5.2 (1)	−6.3 (3)	−8.1 (4)
PPD	−8.2 (1)	−6.9 (1)	−8.4 (0)	−6.9 (0)	−5.6 (0)	−7.7 (1)

[a] ATP-binding pocket of the receptor.
[b] VEGF binding site of the receptor.

3.4. VEGFR2 and AQP1 as potential targets of Rh2

To screen for the possible targets of Rh2 and PPD, molecular docking was performed. A key driver of angiogenesis is the interaction between VEGF and VEGFR2. For the first time, the interaction of Rh2 and PPD with VEGFR2 was studied. VEGFR2 has two major binding sites, the ATP-binding pocket and the VEGF-binding site (Fig. 5B). The extracellular domain of VEGFR2 consists of seven immunoglobulin (Ig) homology domains; D2-3 domains have the highest affinity for VEGF and D4-7 reduce binding affinity by about 10 fold, playing role in regulating the activation and function of the

transmembrane domain, intracellular domain and the ATP-binding pocket of VEGFR2. Molecular docking of S−Rh2 with (**C**) VEGF-binding site and (**D**) the ATP-binding pocket of VEGFR2, and the dose-response curves relating to the action of (**E**) bevacizumab, (**F**) VEGF and S−Rh2 with or without VEGF in the VEGF bioassay system are shown, (**G**) Schematic structure of a monomer AQP1 showing transmembrane domains (M1-M6), loops B and E responsible for water transport and loop D. Molecular docking of (**H**) Rh2 and (**I**) PPD in AQP1 and molecular docking of (**J**) Rh2 and PPD in AQP5. Rh2 makes two H-bonds with HIS-67 and VAL-72 of loop B (water pore).

receptor [38]. The intracellular domain of VEGFR2 is responsible for the kinase activity and downstream signaling. Small-molecule kinase inhibitors such as sunitinib compete with ATP and interact with the ATP-binding pocket of the intracellular domain [39]. Adjacent to this orthosteric ATP-binding site, there is an allosteric site [40]. As shown in Table 1, both Rh2 and PPD were predicted to have a better interaction with the ATP-binding pocket than with the receptor. Despite a good binding score of PPD, given the U-shaped dose-response curve of PPD on loop formation of HUVEC, it is difficult to conclude whether this interaction is inhibitory or stimulatory.

Fig. 5C and D show the interaction sites of Rh2 with VEGF-binding site and the ATP-binding pocket of VEGFR2, respectively. To test the interaction of S−Rh2 with VEGFR2 *in vitro*, a VEGF bioassay was performed. In this assay, upon the activation of VEGFR2 with its ligand, the cells luminesce and in the presence of an inhibitor such as bevacizumab, the luminescence is inhibited. In this assay, bevacizumab, which was used in the presence of VEGF, showed an IC_{50} of 0.11 μg/mL (Fig. 5E). S−Rh2 was used with no VEGF to see if it has stimulatory action on the receptor. In this state, a steady luminescence was detected except at 100 μM, a highly cytotoxic concentration, which could be responsible for reduced luminescence. S−Rh2, alone did not affect the activation of the receptor, but in the presence of VEGF, S−Rh2 shifted the dose-response curve of VEGF to right (Fig. 5F), indicating that S−Rh2 potentially acted as an allosteric modulator of the receptor. Allosteric ligands bind to distinct sites distant from the orthosteric site, change the conformation of the receptor and change the efficacy of the orthosteric ligands or function of the receptor [40]. Our preliminary studies have not shown whether S−Rh2 changes the affinity of VEGF or the function of the receptor, but we have shown that S−Rh2 in the presence of high concentrations of VEGF (EC_{75}), reduced the activation of VEGFR2. This could be particularly important in the hypoxic regions of a tumour when angiogenesis is occurring, and high levels of VEGF exist.

Furthermore, molecular docking was performed with four members of the aquaporin family for which a human crystal structure is published: AQP1, AQP2, AQP4 and AQP5. AQPs have a homo-tetramer structure where each monomer is responsible for the transport of water. Each monomer consists of six transmembrane domains (M1-M6) and three loops (B, D and E) (Fig. 5G). Loops B and E are responsible for water transport function of the channel [41]. Fig. 5H−J shows the molecular docking of Rh2 and PPD into AQP1 and AQP5. Rh2 had good binding scores with both AQP1 and AQP5, with binding scores of −8.1 kJ/mol (Table 1). AQP1 and AQP5 play roles in proliferation, migration, invasion and angiogenesis (reviewed in [2,11]). Both of these AQPs localize at the leading edge of a migrating cell and facilitate cell migration. With AQP1, Rh2 made two H-bonds at HIS-67 and VAL-72 (6H) of loop B (water pore) [41]. With AQP5, it made 4 H-bonds at M2, loop B (Pro 795, Arg-819 (2), and GLN-814. PPD had a better binding score with AQP1 (−8.4 kJ/mol) (Table 1). However, molecular docking showed no H-bonds between the two molecules which might suggest a loose binding compared to that of Rh2. With AQP5, PPD showed a single H-bond with ASN-961 in M6.

As shown in Fig. 5H−J, both Rh2 and PPD showed a better blocking of AQP1, fitting inside the water channel and completely block the passage of water. In the case of AQP5, though the binding scores and number of H-bonds are encouraging, the molecules seem to attach to one side of the water channel and leaving the water passage open (Fig. 5J). Functional assays are required to confirm these *in silico* findings. In comparison, Rg3 had a better binding score with AQP1 (−9.4 kJ/mol) [9]. Binding score of Rh2 and PPD was also weaker than those of other known blockers of AQP1 with saponin structure, such as bacopaside I and II [20]. Using oocyte expression assay, we showed stereoselectivity of Rg3 in blocking AQP1 water channel; SRg3 was a selective blocker of AQP1 [9]. Whether the epimers of Rh2 and PPD have a similar stereoselectivity needs further investigations. Furthermore, in molecular docking studies, Rg3 was more selective for AQP1 and did not show a good binding score with AQP5. Considering the current results, it is possible to conclude that upon administration of Rg3 and production of its metabolites, these ginsenoside could work together and contribute to the observed anti-cancer activities of Rg3. Blocking the water channel function of AQP1 may have an immediate role in inhibition of loop formation and anti-angiogenic effects of Rh2.

4. Conclusion

In conclusion, we have shown that metabolites of Rg3 are more potent anti-proliferative agents than Rg3. They are potential inducers of S-phase arrest and necroptosis in MDA-MB-231 and inducers of G0/G1 arrest and apoptosis in HUVEC. HUVEC was a more sensitive target for the anti-proliferative action of these molecules, a finding relevant to their anti-angiogenic activity. Our current results showed that Rh2 and PPD had a more potent antiangiogenic action than anti-proliferative action on tumour cells. Angiogenesis and tumour cell proliferation are both interdependent factors in tumour progression. The efficacy of these molecules on other breast cancer cell lines should be further studied to better demonstrate potentials of these molecules as anticancer and antiangiogenic agents. S−Rh2 was a most potent anti-angiogenic agent with allosteric modulatory action on VEGFR2 function. Rh2 and PPD have the potential of blocking AQP1 and AQP5. Altogether, these data suggest that metabolites of Rg3 could potentially increase the anti-cancer properties of Rg3, *in vivo*.

Single or combination of these molecules could be considered as potential anti-cancer treatment options for future studies. It should be noticed that since ginsenosides are saponins, there is a potential risk for non-specific cell lysis at high concentrations. Dose optimisation and validation studies are required to find and apply the doses with the highest efficacy and lowest adverse reactions.

Funding

This research was funded by the Margaret Elcombe Research Fellowship, The Hospital Research Foundation.

Declaration of competing interest

The authors declare no conflict of interest.

Appendix A. Supplementary data

Supplementary data to this article can be found online at https://doi.org/10.1016/j.jgr.2021.05.008.

References

[1] Nakhjavani M, Hardingham JE, Palethorpe HM, Tomita Y, Smith E, Price TJ, et al. Ginsenoside Rg3: potential molecular targets and therapeutic indication in metastatic breast cancer. Medicines 2019;6(1):17.
[2] Nakhjavani M, Smith E, Townsend AR, Price TJ, Hardingham JE. Anti-angiogenic properties of ginsenoside Rg3. Molecules 2020;25(21):4905.
[3] Pan L, Zhang T, Sun H, Liu G. Ginsenoside Rg3 (shenyi capsule) combined with chemotherapy for digestive system cancer in China: a meta-analysis and systematic review. Evid Based Complement Alternat Med 2019;2019:2417418.
[4] Lu P, Su W, Miao ZH, Niu HR, Liu J, Hua QL. Effect and mechanism of ginsenoside Rg3 on postoperative life span of patients with non-small cell lung cancer. Chin J Integr Med 2008;14(1):33−6.

[5] Zhou B, Yan Z, Liu R, Shi P, Qian S, Qu X, et al. Prospective study of transcatheter arterial chemoembolization (TACE) with ginsenoside Rg3 versus TACE alone for the treatment of patients with advanced hepatocellular carcinoma. Radiology 2016;280(2):630–9.
[6] Li Y, Wang Y, Niu K, Chen X, Xia L, Lu D, et al. Clinical benefit from EGFR-TKI plus ginsenoside Rg3 in patients with advanced non-small cell lung cancer harboring EGFR active mutation. Oncotarget 2016;7(43):70535–45.
[7] Xie HT, Wang GJ, Sun JG, Tucker I, Zhao XC, Xie YY, et al. High performance liquid chromatographic-mass spectrometric determination of ginsenoside Rg3 and its metabolites in rat plasma using solid-phase extraction for pharmacokinetic studies. J Chromatogr B Analyt Technol Biomed Life Sci 2005;818(2):167–73.
[8] Peng M, Li X, Zhang T, Ding Y, Yi Y, Le J, et al. Stereoselective pharmacokinetic and metabolism studies of 20(S)- and 20(R)-ginsenoside Rg3 epimers in rat plasma by liquid chromatography-electrospray ionization mass spectrometry. J Pharm Biomed Anal 2016;121:215–24.
[9] Nakhjavani M, Palethorpe HM, Tomita Y, Smith E, Price TJ, Yool AJ, et al. Stereoselective anti-cancer activities of ginsenoside Rg3 on triple negative breast cancer cell models. Pharmaceuticals 2019;12(3):117.
[10] Nakhjavani M, Smith E, Yeo K, Palethorpe HM, Tomita Y, Price TJ, et al. Anti-angiogenic properties of ginsenoside Rg3 epimers: in vitro assessment of single and combination treatments. Cancers 2021;13(9):2223.
[11] De Ieso ML, Yool AJ. Mechanisms of aquaporin-facilitated cancer invasion and metastasis. Front Chem 2018;6:135.
[12] Smith E, Palethorpe HM, Tomita Y, Pei JV, Townsend AR, Price TJ, et al. The purified extract from the medicinal plant bacopa monnieri, bacopaside II, inhibits growth of colon cancer cells in vitro by inducing cell cycle arrest and apoptosis. Cells 2018;7(7):81.
[13] Paltoglou S, Das R, Townley SL, Hickey TE, Tarulli GA, Coutinho I, et al. Novel androgen receptor coregulator GRHL2 exerts both oncogenic and anti-metastatic functions in prostate cancer. Cancer Res 2017;77(13):3417–30.
[14] Tomita Y, Palethorpe HM, Smith E, Nakhjavani M, Townsend AR, Price TJ, et al. Bumetanide-derived aquaporin 1 inhibitors, AqB013 and AqB050 inhibit tube formation of endothelial cells through induction of apoptosis and impaired migration in vitro. Int J Mol Sci 2019;20(8):1818.
[15] Palethorpe HM, Smith E, Tomita Y, Nakhjavani M, Yool AJ, Price TJ, et al. Bacopasides I and II act in synergy to inhibit the growth, migration and invasion of breast cancer cell lines. Molecules 2019;24(19):3539.
[16] Mosnier LO, Griffin JH. Inhibition of staurosporine-induced apoptosis of endothelial cells by activated protein C requires protease-activated receptor-1 and endothelial cell protein C receptor. Biochem 2003;373(1):65–70.
[17] Zinonos I, Labrinidis A, Liapis V, Hay S, Panagopoulos V, Denichilo M, et al. Doxorubicin overcomes resistance to drozitumab by antagonizing Inhibitor of Apoptosis Proteins (IAPs). Anticancer Res 2014;34(12):7007–20.
[18] PubChem. PubChem compound summary for CID 119307. Ginsenoside Rh2. NCBI [Internet]. 2020 Nov [cited 2020 Nov 11]. 2020. Available from: https://pubchem.ncbi.nlm.nih.gov/compound/Ginsenoside-Rh2.
[19] PubChem. PubChem compound summary for CID 11213350 (20S)-Protopanaxadiol. NCBI [Internet]. 2020 Nov [cited 2020 Nov 11]. 2020. Available from: https://pubchem.ncbi.nlm.nih.gov/compound/20S_-Protopanaxadiol.
[20] Pei JV, Kourghi M, De Ieso ML, Campbell EM, Dorward HS, Hardingham JE, et al. Differential inhibition of water and ion channel activities of mammalian aquaporin-1 by two structurally related bacopaside compounds derived from the medicinal plant bacopa monnieri. Mol Pharmacol 2016;90(4):496–507.
[21] Zhu S, Liu X, Xue M, Li Y, Cai D, Wang S, et al. 20(S)-ginsenoside Rh2 induces caspase-dependent promyelocytic leukemia-retinoic acid receptor A degradation in NB4 cells via Akt/Bax/caspase9 and TNF-α/caspase8 signaling cascades. J Ginseng Res 2020;45(2):295–304.
[22] Xia T, Zhang J, Zhou C, Li Y, Duan W, Zhang B, et al. 20(S)-Ginsenoside Rh2 displays efficacy against T-cell acute lymphoblastic leukemia through the PI3K/Akt/mTOR signal pathway. J Ginseng Res 2020;44(5):725–37.
[23] Yang J, Yuan D, Xing T, Su H, Zhang S, Wen J, et al. Ginsenoside Rh2 inhibiting HCT116 colon cancer cell proliferation through blocking PDZ-binding kinase/T-LAK cell-originated protein kinase. J Ginseng Res 2016;40(4):400–8.
[24] Liu J, Shimizu K, Yu H, Zhang C, Jin F, Kondo R. Stereospecificity of hydroxyl group at C-20 in antiproliferative action of ginsenoside Rh2 on prostate cancer cells. Fitoterapia 2010;81(7):902–5.
[25] Usami Y, Liu Y-N, Lin A-S, Shibano M, Akiyama T, Itokawa H, et al. Antitumor agents. 261. 20 (S)-protopanaxadiol and 20 (S)-protopanaxatriol as anti-angiogenic agents and total assignment of 1H NMR spectra. J Nat Prod 2008;71(3):478–81.
[26] Choi S, Kim TW, Singh SV. Ginsenoside Rh2-mediated G1 phase cell cycle arrest in human breast cancer cells is caused by p15 Ink4B and p27 Kip1-dependent inhibition of cyclin-dependent kinases. Pharm Res 2009;26(10):2280–8.
[27] Snyder AG, Hubbard NW, Messmer MN, Kofman SB, Hagan CE, Orozco SL, et al. Intratumoral activation of the necroptotic pathway components RIPK1 and RIPK3 potentiates antitumor immunity. Sci Immunol 2019;4(36).
[28] Shlomovitz I, Speir M, Gerlic M. Flipping the dogma—phosphatidylserine in non-apoptotic cell death. Cell Commun Signal 2019;17(1):1–12.
[29] Pietkiewicz S, Schmidt JH, Lavrik IN. Quantification of apoptosis and necroptosis at the single cell level by a combination of Imaging Flow Cytometry with classical Annexin V/propidium iodide staining. J Immunol Methods 2015;423:99–103.
[30] Su Z, Yang Z, Xu Y, Chen Y, Yu Q. Apoptosis, autophagy, necroptosis, and cancer metastasis. Mol Cancer 2015;14(1):48.
[31] Gong Y, Fan Z, Luo G, Yang C, Huang Q, Fan K, et al. The role of necroptosis in cancer biology and therapy. Mol Cancer 2019;18(1):1–17.
[32] Han W, Li L, Qiu S, Lu Q, Pan Q, Gu Y, et al. Shikonin circumvents cancer drug resistance by induction of a necroptotic death. Mol Cancer Ther 2007;6(5):1641–9.
[33] Xuan Y, Hu X. Naturally-occurring shikonin analogues—a class of necroptotic inducers that circumvent cancer drug resistance. Cancer Lett 2009;274(2):233–42.
[34] Fu Z, Deng B, Liao Y, Shan L, Yin F, Wang Z, et al. The anti-tumor effect of shikonin on osteosarcoma by inducing RIP1 and RIP3 dependent necroptosis. BMC Cancer 2013;13(1):1–10.
[35] Wang X, Xia HY, Qin HY, Kang XP, Hu HY, Zheng J, et al. 20 (S)-protopanaxadiol induces apoptosis in human umbilical vein endothelial cells by activating the PERK-eIF2alpha-ATF4 signaling pathway. J Cell Biochem 2019;120(4):5085–96.
[36] Zhang XP, Li KR, Yu Q, Yao MD, Ge HM, Li XM, et al. Ginsenoside Rh2 inhibits vascular endothelial growth factor-induced corneal neovascularization. FASEB J 2018;32(7):3782–91.
[37] Tomita Y, Dorward H, Yool AJ, Smith E, Townsend AR, Price TJ, et al. Role of aquaporin 1 signalling in cancer development and progression. Int J Mol Sci 2017;18(2):299.
[38] Brozzo MS, Bjelić S, Kisko K, Schleier T, Leppänen V-M, Alitalo K, et al. Thermodynamic and structural description of allosterically regulated VEGFR-2 dimerization. Blood 2012;119(7):1781–8.
[39] Christensen J. A preclinical review of sunitinib, a multitargeted receptor tyrosine kinase inhibitor with anti-angiogenic and antitumour activities. Ann Oncol 2007;18:x3–10.
[40] De Smet F, Christopoulos A, Carmeliet P. Allosteric targeting of receptor tyrosine kinases. Nat Biotechnol 2014;32(11):1113–20.
[41] Yool AJ, Brown EA, Flynn GA. Roles for novel pharmacological blockers of aquaporins in the treatment of brain oedema and cancer. Clin Exp Pharmacol Physiol 2010;37(4):403–9.